INSTITUTE OF PHYSICS PUBLISHING JOURNAL OF OPTICS A: PURE AND APPLIED OPTICS

J. Opt. A: Pure Appl. Opt. **7** (2005) S23–S31 doi:10.1088/1464-4258/7/2/003

Electric and magnetic properties of sub-wavelength plasmonic crystals

Gennady Shvets[1] **and Yaroslav A Urzhumov**

Physics Department, University of Texas at Austin, Austin, TX 78712, USA

E-mail: gena@physics.utexas.edu

Received 14 July 2004, accepted for publication 1 December 2004
Published 20 January 2005
Online at stacks.iop.org/JOptA/7/S23

Abstract

Electromagnetic properties of a new class of two-dimensional periodic nanostructured materials, sub-wavelength plasmonic crystals (SPCs), are investigated. An SPC is a periodic lattice of metallic inclusions with negative dielectric permittivity $\epsilon < 0$ imbedded in a dielectric host with $\epsilon_h > 0$, with the lattice period much smaller than the wavelength of light. It is found that two types of propagating electromagnetic waves are supported by SPCs: (a) scale-invariant modes whose dispersion relation is almost independent of the lattice period, and (b) scale-dependent narrow-band resonances whose dispersion strongly depends on the lattice period. The scale-invariant modes are accurately described using a frequency-dependent quasi-static dielectric permittivity $\epsilon_{qs}(\omega)$ and a vacuum magnetic permittivity $\mu = 1$. The scale-dependent resonances exist inside narrow frequency bands where they can have a modified magnetic permittivity $\mu \neq 1$. Magnetic properties originate from the non-vanishing magnetic moment produced by the currents inside any given plasmonic inclusion due to the close proximity of the adjacent inclusions. Applications of SPCs to the development of novel left-handed metamaterials in the optical range are discussed. A new paradigm of the SPC-based surface-enhanced Raman scattering is also introduced.

Keywords: sub-wavelength plasmonic crystals, electromagnetic properties, left-handed metamaterials, periodic nanostructured materials

(Some figures in this article are in colour only in the electronic version)

1. Introduction and motivation

The ability of periodic dielectric structures to significantly alter the propagation of light has been realized with the introduction of a photonic crystal [1–4]. To maximize the effect of the structure on the dispersion properties of propagating electromagnetic waves, the crystal period is typically of the order of the light wavelength. Light propagation is affected in several ways: through creation of the stop-bands (band gaps) separating adjacent propagation bands, group velocity reduction near the propagation band edge, generation of cavity states localized near a defect [3], polarization-dependent birefringence [5], and extreme anisotropy with respect to propagation direction [6]. Applications of dielectric photonic crystals (PCs) include low-loss fibres [7], microcavity lasers [8], band-edge quantum cascade lasers, cavity quantum electrodynamics, and development of novel quarter waveplates [5].

Several even more exotic applications of dielectric PCs have been recently suggested: development of the so-called left-handed (or negative index) materials, flat photonic lenses, and sub-wavelength imaging [9] capable of exceeding the diffraction limit. Since the resolution of any PC-based lens is limited by the crystal period [10], beating the diffraction limit requires using a PC with a sub-wavelength period [11]. In addition to dielectric PCs, a new class of metallic photonic crystals (MPCs) has recently drawn attention because of their wide bandgap for short wavelengths [12] and the ability to

[1] Author to whom any correspondence should be addressed.

act as efficient filters of electromagnetic radiation [13, 14]. Even more exciting electromagnetic phenomena occurring in MPCs are the existence of left-handed waves [15] which can be used for sub-wavelength imaging [16] and extreme field enhancement by arrays of metallic nanorods [17] which can be used for surface-enhanced Raman scattering (SERS). Since all these applications require sub-wavelength scale MPCs, it is important to understand and classify the types of electromagnetic (EM) waves supported by such structures.

Moreover, in the optical/UV frequency range metals behave very differently than at the longer wavelengths. Because of the strong (plasma-like) frequency dependence of the metallic dielectric permittivity $\epsilon(\omega)$ in that frequency range, metallic inclusions are referred to as *plasmonic*. Accounting for the dispersion of $\epsilon(\omega)$ becomes necessary, even further complicating an already challenging task of calculating the detailed photonic bands of a PC. To address this challenge, we develop a new technique for calculating the dispersion properties of sub-wavelength plasmonic crystals (SPCs). This technique is based on the assumption $\omega d/c \ll 1$, where d is the crystal period and c is the speed of light in vacuum. However, we go beyond the traditional electric dipole approximation [18, 19] and demonstrate how higher-multipole plasmonic resonances can produce magnetic moments of a plasmonic inclusion and give rise to electromagnetic waves with a negative magnetic permeability. When metals are used as negative ϵ inclusions, the typical lattice period that satisfies the 'sub-wavelength' criterion is under 50 nm. Therefore, metallic SPCs are necessarily nanostructured. Because the focus of this work is on plasmonic structures, the metallic inclusions will be occasionally referred to as nanorods or nanoparticles.

By examining numerically obtained solutions of Maxwell's equations for the SPC, we identify two classes of waves supported by an SPC: (a) hybridized dipole modes that are characterized by a quasi-static period-independent dielectric permittivity $\epsilon_{\rm qs}(\omega)$, and (b) hybridized higher-multipole resonances (HMRs) that depend on the crystal period d. Two types of dipole modes are identified: almost dispersionless (non-propagating) bulk plasmons (BPs) satisfying the $\omega(\vec{k}) \equiv \omega_i^{(\rm c)}$ dispersion relation (where $\omega_i^{(\rm c)}$ are multiple zeros of $\epsilon_{\rm qs}$), and propagating plasmon polaritons (PPs) satisfying the $\vec{k}^2c^2 = \omega^2\epsilon_{\rm qs}(\omega)$ dispersion relation. The effective medium dielectric permittivity $\epsilon_{\rm qs}$ calculated from the quasi-static electric dipole theory (QSED) [18, 19] is found to be highly accurate in predicting wave propagation even for SPCs with the period as large as $\lambda/2\pi$. Dipole mode propagation bands are 'sandwiched' between multiple resonance $\omega_i^{(\rm r)}$ and the cut-off $\omega_i^{(\rm c)}$ frequencies of the SPC. For two-dimensional SPCs with a high lattice symmetry (square and hexagonal) a duality condition expressing a simple one-to-one correspondence between the resonant and cut-off frequencies is discovered.

The new HMR propagation bands are discovered inside the frequency intervals where $\epsilon_{\rm qs} < 0$ and, according to the QSED theory, propagation is prohibited. HMR bands should not be confused with the usual high-order Brillouin zones of a photonic crystal because the latter do not satisfy the $d \ll \lambda$ condition. One HMR band defines the frequency range for which the sub-wavelength photonic crystal behaves as a double-negative metamaterial that can be described by the negative effective permittivity $\epsilon_{\rm eff} < 0$ and permeability $\mu_{\rm eff} < 0$ [20]. Negative $\mu_{\rm eff}$ result from the induced magnetic moment inside each nanoparticle by high-order multipole electrostatic resonances of its neighbours.

2. Propagation bands in a two-dimensional sub-wavelength plasmonic crystal: general theory and numerical simulations

For the remainder of this paper we concentrate on transverse magnetic (TE), also known as p-polarized, electromagnetic waves propagating in the x–y plane of a two-dimensional photonic crystal. The photonic crystal is assumed to be a square array with period d of cylindrical inclusions (rods of radius R infinitely extended in the z-direction) with dielectric permittivity ϵ imbedded in a host material with dielectric permittivity $\epsilon_{\rm h} \equiv 1$. The non-vanishing em field components are H_z, E_x, and E_y. Propagation bands can be obtained by solving the nonlinear eigenvalue equation for H_z:

$$-\vec{\nabla}\cdot\left(\frac{1}{\epsilon(\omega,\vec{x})}\vec{\nabla}H_z\right) = \frac{\omega^2}{c^2}H_z, \tag{1}$$

where H_z satisfies phase-shifted boundary conditions at the edges of the elementary cell:

$$\begin{aligned} H_z(d/2, y) &= \mathrm{e}^{\mathrm{i}k_x d}H_z(-d/2, y),\\ H_z(x, d/2) &= \mathrm{e}^{\mathrm{i}k_y d}H_z(x, -d/2). \end{aligned} \tag{2}$$

The electric field of the wave is given by $\vec{E}(\vec{x}) = -\mathrm{i}[c/\omega\epsilon(\vec{x})]\vec{e}_z \times \vec{\nabla}H_z$. $\epsilon(\vec{x}) = \epsilon_{\rm h}$ outside and $\epsilon(\vec{x}) = \epsilon(\omega)$ inside the inclusion. The dielectric permittivity $\epsilon(\omega, \vec{x})$ is assumed to be piecewise constant: $\epsilon(\omega, \vec{x}) = \epsilon(\omega)\theta(\vec{x}) + \epsilon_{\rm h}[1 - \theta(\vec{x})]$, where $\theta(\vec{x})$ is a Heaviside function equal to 1 inside the plasmonic cylinder and 0 outside. Solving equation (1) yields the dispersion relation ω versus $\vec{k} = k_x\vec{e}_x + k_y\vec{e}_y$, where $-\pi/d < k_x, k_y < \pi/d$. Due to band folding, multiple Brillouin zones (propagation bands) separated by stop-bands are revealed. Thus $\omega^{(n)2}$, where n labels the Brillouin zones (BZs), is a multi-valued function of $\vec{k}$ and crystal period d. The band edge $\vec{k} = 0$ (Γ-point) corresponds to periodic boundary conditions on H_z.

There is an important difference in the electromagnetic properties of dielectric (with frequency-independent $\epsilon(\omega) \equiv \epsilon_i$) and plasmonic (with $\epsilon(\omega) \equiv 1 - \omega_{\rm p}^2/\omega^2$) photonic crystals in the limit of $d \to 0$. For small $|\vec{k}| \ll \pi/d$ EM waves propagating through the former can be described using the effective medium d-independent dielectric permittivity $\epsilon_{\rm eff}$ only for the lowest BZ. For the upper BZs the wave frequencies scale inversely proportionally with d. On the other hand, there are two classes of waves supported by a plasmonic PC:

(i) Non-resonant waves (dipole modes) which exist far from electrostatic resonances, and are described by the dispersion relation $k^2 = \epsilon_{\rm eff}(\omega)\omega^2/c^2$, where for $d \to 0$ $\epsilon_{\rm eff} = \epsilon_{\rm qs}(\omega)$. The quasi-static dielectric permittivity $\epsilon_{\rm qs}(\omega)$ is calculated using the conventional QSED theory [18, 19] as explained in section 3.

(ii) Higher-multipole resonances with the dispersion relation $\omega \equiv \omega(k^2d^2)$.

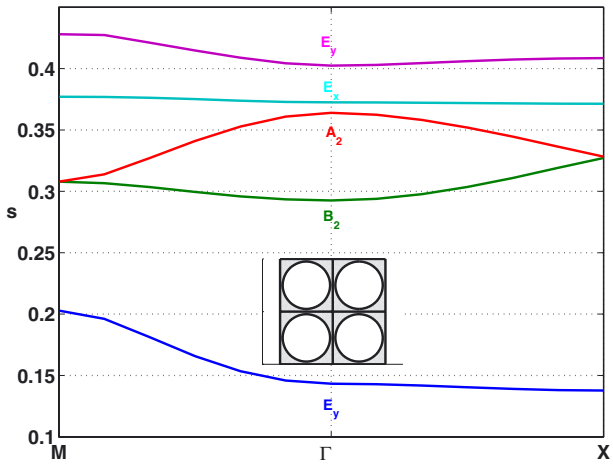

Figure 1. Electrostatic resonances of the square lattice SPC consisting of almost-touching plasmonic cylinders with $R/d = 0.45$ (shown as an inset). Vertical axis: $s = 1/[1 - \epsilon(\omega)] \equiv \omega^2/\omega_p^2$, horizontal axis: wavenumber. Scanned eigenvalue range: $0 < s < 0.45$.

Although these waves are predominantly electrostatic, they can excite a finite magnetic moment inside the plasmonic inclusions. These profound differences between dielectric and plasmonic periodic structures are caused by the *electrostatic resonances*, introduced in section 2.1.

In the rest of the paper we concentrate on the specific SPC shown as an inset in figure 1: a square lattice of round ($R = 0.45d$) almost-touching *plasmonic* cylinders with the frequency-dependent dielectric permittivity $\epsilon(\omega) = 1 - \omega_p^2/\omega^2$ characteristic of a collision-free electron gas described by the Drude model. The cylinders are separated by the lattice period $d = c/\omega_p$.

2.1. Electrostatic resonances in sub-wavelength plasmonic crystals

For a sub-wavelength rod the rhs of equation (1) can be neglected as long as $\omega^2 d^2/c^2 \ll 1$ (because $\nabla H_z \sim H_z/d$). Hence, the total magnetic field satisfying equation (1) can be expressed as $H_z = H_{qs} + H_1$, where H_{qs} satisfies the generalized nonlinear eigenvalue equation (for a real number $\epsilon(\omega)$ and, therefore, implicitly for ω):

$$-\vec{\nabla}\cdot\left(\epsilon^{-1}\vec{\nabla}H_{qs}\right) = 0, \tag{3}$$

where H_{qs} satisfies the phase-shifted boundary conditions described by equation (2). Equation (3) is an eigenvalue equation only in the sense of having non-trivial solutions only for certain values of ϵ. The $\vec{k}$-dependent eigenvalues $\epsilon_j^{(r)}$ of the equation (3) form a discrete spectrum: $1 < j < \infty$, and the superscript (r) denotes the resonance. The frequency-dependent $\epsilon_j^{(r)}$ defines the mode frequency $\omega_j^{(r)}$ which can be used to calculate H_1, assumed to be a small correction (of order $\omega^2 d^2/c^2$) to H_{qs}. The inhomogeneous equation for H_1 is

$$-\vec{\nabla}\cdot\left(\epsilon^{-1}\vec{\nabla}H_1\right) = \frac{\omega^2}{c^2}H_{qs}, \tag{4}$$

where H_1 also satisfies equations (2).

It can be shown that the em waves with frequencies close to $\omega_j^{(r)}(\vec{k})$ are predominantly electrostatic. Indeed, the electric field $\vec{E} = -i[c/\omega\epsilon]\vec{e}_z \times \vec{\nabla}H_z$ can be separated into the electrostatic and solenoidal components: $\vec{E} = \vec{E}_{es} + \vec{E}_{sol}$, where $\vec{E}_{es} = -i[c/\omega\epsilon]\vec{e}_z \times \vec{\nabla}H_{qs}$ and $\vec{E}_{sol} = -i[c/\omega\epsilon]\vec{e}_z \times \vec{\nabla}H_1$. From $|H_{qs}| \gg |H_1|$ it follows that $|E_{qs}| \gg |E_{sol}|$. It is straightforward to show that $\vec{\nabla} \times \vec{E}_{es} = 0$, so that the electric field is indeed predominantly electrostatic. Thus, it can be expressed as the gradient of an electrostatic potential ϕ: $\vec{E}_{qs} = -\vec{\nabla}\phi$. Because in the electrostatic limit Maxwell's equations simplify to $\vec{\nabla}\cdot(\epsilon\vec{E}) = 0$, two equations for ϕ and H_z are simultaneously satisfied for a sub-wavelength plasmonic crystal:

$$-\vec{\nabla}\cdot\left(\epsilon^{-1}\vec{\nabla}H_{qs}\right) = 0 \qquad \text{and} \qquad -\vec{\nabla}\cdot\left(\epsilon\vec{\nabla}\phi\right) = 0. \tag{5}$$

Equations (5) will be used in section 3.3 to derive a useful duality relationship between resonances and cut-offs of electromagnetic waves propagating in an SPC. Note that the electrostatic assumption can only be used in close proximity of the resonant frequencies $\omega_j^{(r)}$. Away from resonances a different procedure (described in section 3) must be used to describe the propagation of em waves in an SPC. The perturbative calculation of H_1 according to equation (4) also loses validity away from the electrostatic resonances.

Electrostatic resonances for the specific SPC are calculated for a range of propagation wavenumbers $\vec{k}$ inside the Brillouin zone by solving the eigenvalue equation (5) for ϕ. For computational convenience equation (5) is recast in the form of

$$\vec{\nabla}\cdot\left[\theta(\vec{x})\vec{\nabla}\phi_i\right] = s_i\nabla^2\phi_i, \tag{6}$$

where ϕ_i are the potential functions corresponding to electrostatic resonances satisfying the periodically phase-shifted boundary conditions analogous to equation (2), and $s_i = (\omega_i^{(r)}/\omega_p)^2$. The dependence of s_i on the wavenumber is presented in figure 1, where the inset shows four unit cells of the SPC. The wavenumber $\vec{k}$ is labelled in figure 1 according to the standard convention: the Γ–X direction is along the x-axis and Γ–M along the diagonal of the SPC. The finite elements code FEMLAB [21] was used to solve equation (6). All eigenvalues were computed to at least fourth decimal accuracy as verified by successive refinements of the computational mesh.

The different curves represent different families of resonances labelled according to their symmetry at the Γ-point ($\vec{k} = 0$). For example, the resonance labelled as B_2 is a quadrupole: its lowest azimuthal dependence is $\phi_i^{(B_2)} \propto \sin 2\theta$ at the Γ-point. Azimuthal dependences of some of the other resonances are: $\phi_i^{(A_2)} \propto \sin 4\theta$ (octupole), $\phi_i^{(E_x)} \propto \cos\theta$, and $\phi_i^{(E_y)} \propto \sin\theta$ (dipoles). Angular dependences of the E-modes are given for $\vec{k} = \delta k\vec{e}_x$, where δkd is infinitesimal. The resonances labelled as E_y and E_x are special because they have a non-vanishing dipole moment, and describe the modes resonantly excited by the uniform $\vec{E} = E_0\vec{e}_y$ or $\vec{E} = E_0\vec{e}_x$ fields, respectively. E_x and E_y are hybridized dipole resonances while the others (e.g. A_2 and B_2) are higher-multipole resonances (HMRs). Note that the wavenumber enters equation (5) only through the boundary conditions, and only through the combinations $k_x d$ and $k_y d$. Therefore, the

dispersion relations for all resonances have ω versus $|\vec{k}|d$ dependences, and, therefore, are period-dependent.

It would be tempting to assume that the propagation curves in figure 1 calculated in the vanishing period limit $\omega^2 d^2/c^2 \ll 1$ accurately describe *all* waves propagating in a finite-d SPC. This turns out not to be the case. Electrostatic calculation is accurate only in close proximity of electrostatic resonances. Away from those resonances the electrostatic assumption is invalid, and other modes emerge. For instance, by numerically solving the full electromagnetic equation (1), we have identified a propagating mode below the lowest (in frequency) electrostatic E_y resonance ($s < 0.14$). That mode merges with the E_y curve for $|\vec{k}| \gg 1/d$.

It is also found, based on the group theoretical analysis of equation (1) explained in section 2.2, that the electromagnetic modes form a doublet at the Γ-point corresponding to the E_x resonance. The degeneracy is removed for finite $\vec{k} = k_x\vec{e}_x$, and the doublet is split into lower and higher frequency modes. The low-frequency mode of the doublet referred to as a bulk plasmon (BP) is x-polarized, practically dispersionless, and has the propagation properties almost identical to the electrostatic E_x mode. The high-frequency mode referred to as the plasmon polariton (PP) is y-polarized and occupies a much wider frequency range than the BP: between the E_x and E_y resonances. For large $|\vec{k}| \gg 1/d$ the PP's frequency approaches that of the E_y resonance, and the dispersion curve of the PP merges with that of E_y. The x- and y-polarized electromagnetic waves are strictly frequency-degenerate at the Γ-point, whereas the approximate electrostatic calculation in figure 1 gives a misleading impression that they are not. Both the BP and the PP are hybridized dipole modes because, as shown in section 3, their fields can be expanded as a sum of hybridized dipole resonances.

Other propagating electromagnetic modes of a finite-period SPC are not frequency-degenerate at the Γ-point. Those modes indeed are the hybridized higher-order multipole resonances. Even for finite-sized nanoparticles, HMR dispersion relations are very accurately described by the dispersion curves shown in figure 1. Electromagnetic properties of HMRs are period-dependent because ω depends on $|\vec{k}|d$.

2.2. *Propagating waves in a sub-wavelength plasmonic crystal: simulation results*

Symmetry considerations are very useful in classifying the electromagnetic modes supported by an SPC. The square lattice of the SPC is invariant with respect to the transformations of the C_{4v} point group [22]. Symmetry arguments can be most readily applied to the highly symmetric Γ-point of the electromagnetic bands corresponding to $\vec{k} = 0$. The eigenmodes of equation (1) satisfy the periodic boundary conditions at the Γ-point. Thus these periodic solutions transform according to one of the irreducible representations (IRREPS) of C_{4v}: four singlets (commonly labelled as A_1, A_2, B_1, and B_2) and one doublet E. The Γ-point solutions can also be labelled according to their IRREPS. Only the doublet E has a non-vanishing dipole moment. Therefore we expect that some of the solutions of equation (1) are non-degenerate

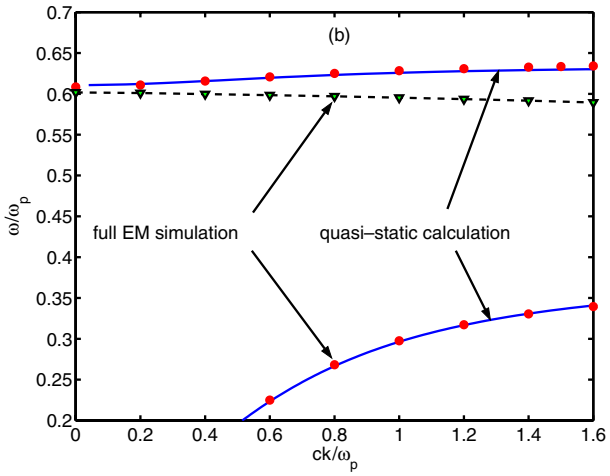

Figure 2. Propagation bands of a sub-wavelength plasmonic crystal with parameters from figure 1 and $d = c/\omega_p$. Circles and triangles: calculated by solving equation (1). Solid curves: predictions of the quasi-static electric dipole theory, $k = \sqrt{\epsilon_{qs}}\omega/c$.

at the Γ-point (singlets) while others are doubly-degenerate (doublets).

By numerically solving equation (1) some of the representative propagation bands have been computed for a range of frequencies $0 < \omega < 0.7\omega_p$ and propagation wavenumbers $\vec{k} = k\vec{e}_x$. The resulting ω versus k dispersion relations are marked by symbols (circles and triangles) in figure 2. The lowest propagation band (circles) starts at the origin and approaches what appears to be a resonance. The electric field of the propagating mode is primarily in the y-direction, and the resonant frequency is close to that of the lower E_y resonance ($\omega = 0.37\omega_p$) in figure 1 at the Γ-point. The two frequencies cannot be expected to exactly coincide because the SPC period, while sub-wavelength, is still finite: $d = c/\omega_p$.

The upper propagation band starts at $\omega \approx 0.61\omega_p$, where it turns out to be a doublet consisting of (i) a non-propagating collective plasmon BP with $\omega(k) \approx 0.61\omega_p$ (not shown due to its flatness in frequency), and (ii) a propagating PP whose dispersion is shown by circles in figure 2. The frequency of the BP coincides with that of the E_x resonance in figure 1. That is so because EM fields of the BP are largely electrostatic ($|E_x| \gg |H_z|$) for all values of k. The propagation band of the PP is very narrow: $0.61\omega_p < \omega < 0.63\omega_p$; it is bounded from above by a resonance at $\omega = 0.63\omega_p$ which coincides with that of the upper E_y resonance in figure 1 at the Γ-point. As explained in section 3, for small $k \ll \pi/d$ these two propagation bands are sufficiently far away from electrostatic resonances to be accurately described by the scale-independent effective dielectric permittivity $\epsilon_{qs}(\omega)$ calculated using QSED theory. The results of the full electromagnetic calculation (circles) closely follow the theoretical curves $k = \sqrt{\epsilon_{qs}}\omega/c$.

The middle propagation band (marked by triangles) corresponds to the electrostatic resonance A_2 shown in figure 1. Wave dispersion in this band cannot be derived from ϵ_{qs} because of its proximity to the octupole resonance. Note that for the A_2 HMR $\partial\omega/\partial k < 0$: its group and phase velocity oppose each other. Such behaviour is also found in negative

refractive index metamaterials which are characterized by the negative effective permittivity $\epsilon_{\rm eff} < 0$ and permeability $\mu_{\rm eff} < 0$ [20]. Section 4 explains the origin of the negative effective magnetic permeability of this wave.

3. Propagation bands removed from electrostatic resonances: quasi-static electric dipole theory

Away from electrostatic resonances, a well established methodology exists for characterizing the frequency-dependent electromagnetic properties of a nanostructure. This is done by introducing a frequency-dependent quasi-static dielectric permittivity $\epsilon_{\rm qs}(\omega)$ of a nanostructure [18, 19]. We refer to this approach as the quasi-static electric dipole (QSED) theory because it takes into account only hybridized dipole resonances of the nanostructure. For the frequencies sufficiently removed from higher-multipole resonances this is a justifiable assumption: dipole scattering by individual particles dominates over the multipolar scattering.

3.1. Quasi-static electric dipole theory

The material-independent $\epsilon_{\rm qs}$ can be obtained [18, 19] by calculating the frequencies and strengths of the dipole-possessing electrostatic resonances, and summing them up with the appropriate weighting factors:

$$\epsilon_{\rm qs} = 1 - p\sum_{i=1}^{N}\frac{F_i}{s - s_i}, \tag{7}$$

where, for the plasmonic rods in vacuum, $s(\omega) = [1 - \epsilon(\omega)]^{-1} = \omega^2/\omega_{\rm p}^2$, $s_i \equiv [1 - \epsilon_i^{(\rm r)}]^{-1}$ is the ith out of $N > 1$ hybridized dipole resonances, F_i its dipole strength calculated below, and $p = \pi R^2/d^2$ is the filling ratio. The electrostatic resonances s_i are found by solving the eigenvalue equation, equation (6), inside the unit cell. Restricting the calculation to long-wavelength modes with $|\vec{k}| \ll \pi/d$, the spatial dispersion of $\epsilon_{\rm qs}$ can be neglected.

The potential eigenfunctions ϕ_i satisfy the following homogeneous conditions at the unit boundaries $(x, y) = (\pm d/2, \pm d/2)$: (a) ϕ_i and its derivatives are periodic; (b) $\phi_i(y = \pm d/2) = 0$; (c) $\partial_x\phi_i(x = \pm d/2) = 0$. Because of the symmetry of the problem, the ϕ_i are periodic throughout the lattice. Physically, these eigenfunctions describe the electric potential distribution when a vanishing ac voltage (with frequency $\omega_i^{(\rm r)}$ such that $\epsilon(\omega) = \epsilon_i$) is applied between $y = \pm d/2$ capacitor plates. The capacitance per unit length in z of such an imaginary capacitor, equal to the ratio of the charge per unit length to the voltage drop, is given by $C = \epsilon_{\rm qs}/4\pi$. Capacitance C becomes infinite for $\omega = \omega_i^{(\rm r)}$ according to equation (7): finite charge induces a vanishing voltage drop $\delta\phi = \phi(y = d/2) - \phi(y = -d/2)$. Note that another periodic eigenfunction $\tilde{\phi}_i$ corresponding to the voltage drop applied between $x = \pm d/2$ plates is obtained by a 90° spatial rotation of ϕ_i.

For frequencies different from $\omega_i^{(\rm r)}$ a finite imposed electric field induces a finite voltage drop $\delta\phi$. It is more convenient to solve the inverse problem and calculate the electric field required to induce a given voltage drop $\delta\phi = d$. Without the plasmonic inclusion the required electric field is $E_0 = 1$, and the resulting potential inside the elementary $d \times d$ square cell is $\phi_0 = y$. With the plasmonic inclusion the electrostatic potential can be expanded as the sum of ϕ_0 and hybridized dipole resonances [19]:

$$\phi(x, y) = \phi_0 + \sum_i \frac{s_i\phi_i(x, y)}{s(\omega) - s_i} \times \frac{\int {\rm d}x\,{\rm d}y\,\phi_0\nabla^2\phi_i^*}{\int {\rm d}x\,{\rm d}y\,\phi_i\nabla^2\phi_i^*}. \tag{8}$$

The electric field $E_y = -\partial_y\phi(x, -d/2)$ at the bottom capacitor plate ($y = -d/2$) can now be calculated from equation (8). Because the total charge per unit length z is $\delta Q = (4\pi)^{-1}\int {\rm d}x\, E_y$, the total capacitance per unit length can be calculated as $C = \delta Q/\delta\phi$. Using equation (7) and that $\epsilon_{\rm qs} = 4\pi C$, it can be shown [19] that the dipole strength F_i is given by

$$F_i = -\frac{s_i}{\pi R^2}\frac{\left|\int {\rm d}x\,{\rm d}y\,\phi_0\nabla^2\phi_i\right|^2}{\int {\rm d}x\,{\rm d}y\,\phi_i^*\nabla^2\phi_i}. \tag{9}$$

From equation (9) it follows that only the resonances with a non-vanishing dipole moment at the Γ-point contribute to $\epsilon_{\rm qs}(\omega)$. For example, the E_y resonances from figure 1 contribute to $\epsilon_{\rm qs}$ while the A_2, B_2, and E_x do not. We conjecture, and later verify, that the quasi-static dielectric permittivity $\epsilon_{\rm qs}(\omega)$ calculated from equations (7), (9) can be used for deriving the dispersion characteristics of y-polarized electromagnetic waves propagating in the x-direction.

The dipole strengths can be significantly simplified for a square lattice of round plasmonic rods. Because the square lattice is invariant with respect to the transformations of the C_{4v} point group [22], all periodic solutions transform according to one of the irreducible representations (IRREPS) of C_{4v}: four singlets (commonly labelled as A_1, A_2, B_1, and B_2) and one doublet E. The electrostatic eigenfunctions with a non-vanishing dipole moment $\phi_i^{(E)}$ and $\tilde{\phi}_i^{(E)}$ have the symmetry of E. By symmetry, inside a given rod each $\phi_i^{(E)}$ can be expanded as the sum of multipoles: $\phi_i^{(E)}(r, \theta) = \sum_{l=0}^{\infty} A_i^{(2l+1)}(r/R)^{2l+1}\sin(2l+1)\theta$. Because ϵ is a piecewise constant function of the radius, and $\nabla^2\phi_i = 0$ inside and outside of the rod, for any ϕ_i we can simplify $\nabla^2\phi_i = \delta(r - R) \times [\partial_r\phi_i(r = R + 0) - \partial_r\phi_i(r = R + 0)]$. By continuity of $\epsilon({\rm r})\partial_r\phi_i$ we can further simplify $\nabla^2\phi_i = \delta(r - R)(\epsilon_i - 1)\partial_r\phi_i(r = R - 0)$. Using the multipole expansion inside the rod one finds that the dipole strength is proportional to the dipole component of $\phi_i^{(E)}$: $F_i = \left(A_i^1\right)^2 / \sum_{l=0}^{\infty}(2l+1)\left(A_i^{2l+1}\right)^2$.

For the plasmonic structure analysed here there are three significantly strong hybridized dipole resonances: ($s_1 = 0.1433$, $F_1 = 0.8909$), ($s_2 = 0.4025$, $F_2 = 0.064$), and ($s_3 = 0.6275$, $F_3 = 0.0366$). In general, there are infinitely many hybridized dipole resonances, most of them clustering around the singular point of $s_i = 1/2$ (or $\omega_i = \omega_{\rm p}/\sqrt{2}$) which corresponds to the resonance of an *isolated* plasmonic rod. The total sum of their dipole strengths can be rigorously shown to be unity: $\sum_{n=1}^{\infty} F_n = 1$. Because $\sum_{n=1}^{3} F_n = 0.992$, we are justified in neglecting weaker dipole resonances and using the strongest three in equation (7) for calculating $\epsilon_{\rm qs}(\omega)$. The potential functions $\tilde{\phi}_i$ of the three strongest dipole resonances (corresponding to the electric field in x-direction) are shown in figures 3(a)–(c). The first resonance is primarily dipolar ($\propto\cos\theta$), while the second one has a significant sextupolar ($\propto\cos 3\theta$) component. Thus, the close proximity of the rods in

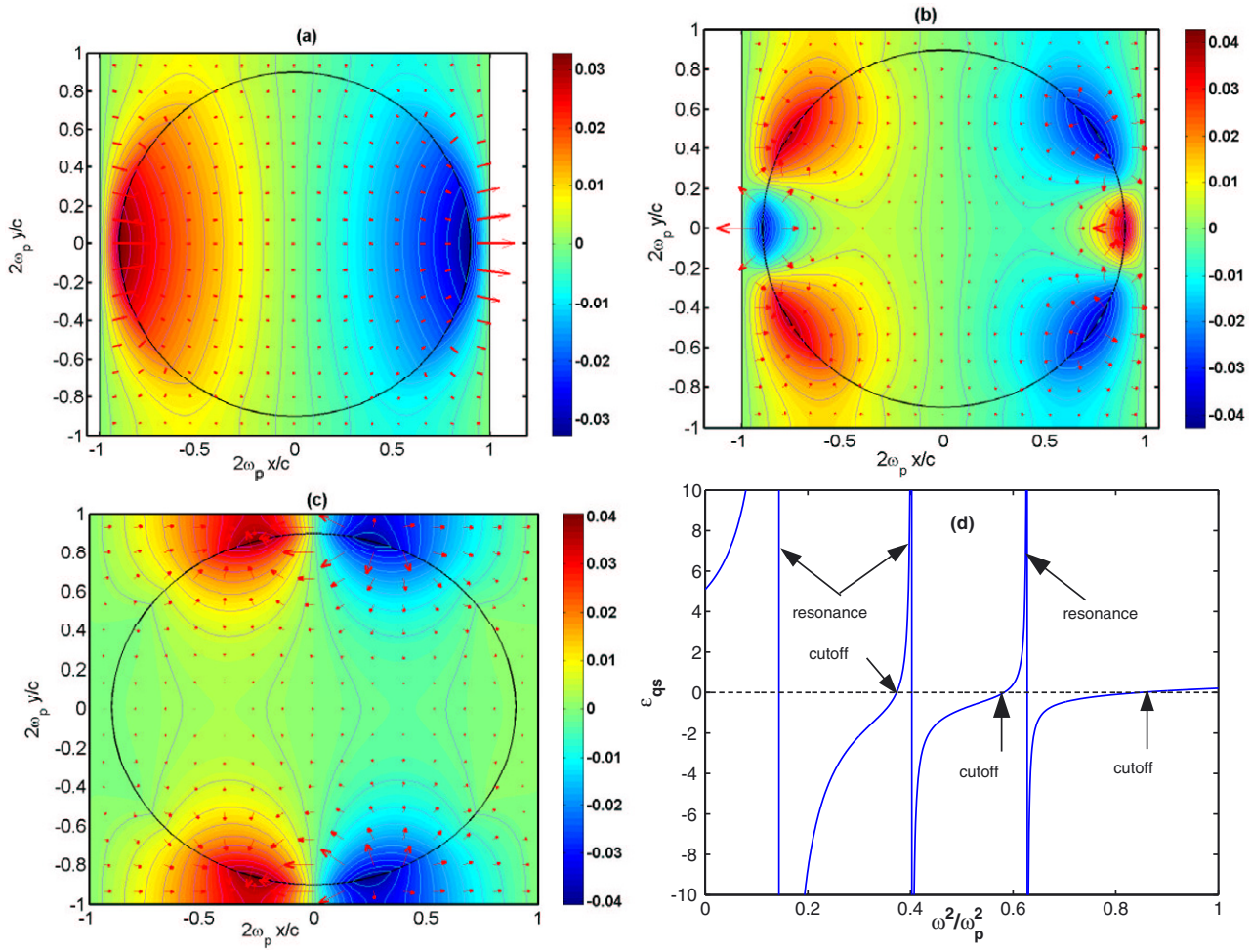

Figure 3. (a)–(c) The potential functions of the three strongest hybridized dipole resonances of the SPC with parameters from figure 1, in the order of decreasing dipole strength (contours) and the corresponding electric field (arrows). (d) Quasi-static dielectric permittivity ϵ_{qs} versus ω calculated from equation (7) using the three strongest resonances. If viewed in greyscale, then in (a) the low-value region is at the right, and the high-value region is at the left; in (b) the low-value regions are at middle-left, top-right and bottom-right, and the high-value regions are at middle-right, top-left and bottom-left; in (c) the low-value regions are at top-right and bottom-right, and the high-value regions are at top-left and bottom-left.

the lattice results in a strong hybridization of the odd multipoles with the dipole. Moreover, the hybridized dipole resonances $\omega_1^{(r)} = 0.38\omega_p$, $\omega_2^{(r)} = 0.63\omega_p$, and $\omega_3^{(r)} = 0.79\omega_p$ occur at the frequencies *controllably* different (through the R/d ratio) from that of an isolated rod, $\omega^{(r)} = \omega_p/\sqrt{2}$. Red-shifting of the strongest dipole resonance of a nanoparticle due to close proximity of other nanoparticles has been observed experimentally [27].

The corresponding quasi-static dielectric permittivity ϵ_{qs} is plotted in figure 3(d) as a function of the frequency ω. Infinities of ϵ_{qs} correspond to electrostatic dipole resonances. In calculating $\epsilon_{qs}(\omega)$ we have neglected the finite damping in the plasmonic rods. If damping is accounted for, the infinities of ϵ_{qs} are removed. Another set of special frequencies $\omega_i^{(c)}$ is the cut-off frequencies for which $\epsilon_{qs}(\omega_i^{(c)}) = 0$. For the structure analysed here there are three such frequencies: $\omega_1^{(c)} = 0.61\omega_p$, $\omega_2^{(c)} = 0.77\omega_p$, and $\omega_3^{(c)} = 0.93\omega_p$. Note that ϵ_{qs} is independent of the SPC periodicity scale d and is only dependent on the geometry (i.e. R/d). Therefore, the quasi-static ϵ_{qs} approach is the effective medium theory which neglects the internal structure the SPC.

3.2. Wave propagation in an SPC

Propagation properties of electromagnetic waves through any medium (including an SPC) characterized by the effective medium $\epsilon_{eff}(\omega)$ can be obtained by solving Maxwell's equations in the medium for space-averaged quantities $\vec{\mathcal{H}}$ and $\vec{\mathcal{E}}$ [23]:

$$\vec{\nabla} \times \vec{\mathcal{E}} = \frac{i\omega}{c}\mu_{eff}\vec{\mathcal{H}}, \qquad \vec{\nabla} \times \vec{\mathcal{H}} = -\frac{i\omega\epsilon_{eff}}{c}\vec{\mathcal{E}}, \tag{10}$$

where the electromagnetic field is assumed to be harmonic in time.

The prescription for calculating the averaged fields for a three-dimensional photonic crystal has been introduced elsewhere [11, 24]. Modifications to those procedures were made in order to adapt them to the two-dimensional problem at hand. Specifically, we assumed that the elementary cell is a cube with height d in the z-direction. Because all physical quantities (electric and magnetic fields) are z-independent, surface integrals over the faces parallel to z are reduced to line integrals. For two dimensions, and assuming that

the elementary cell of the SPC is centred at the origin, the averaged $\vec{\mathcal{E}}$ and $\vec{\mathcal{D}}$ are defined as $\mathcal{E}_y = d^{-1}\int_{-d/2}^{+d/2} \mathrm{d}y\, E_y(x = -d/2, y)$, $\mathcal{E}_x = d^{-1}\int_{-d/2}^{+d/2} \mathrm{d}x\, E_x(x, y = -d/2)$, $\mathcal{D}_y = d^{-1}\int_{-d/2}^{d/2} \mathrm{d}x\, E_y(x, y = -d/2)$, $\mathcal{D}_x = d^{-1}\int_{-d/2}^{d/2} \mathrm{d}y\, E_x(x = -d/2, y)$. Since away from electrostatic resonances an SPC does not exhibit magnetic properties, it is assumed that $\mu_{\mathrm{eff}} = \mathcal{B}_z/\mathcal{H}_z \equiv 1$, where $\mathcal{B}_z = d^{-2}\int \mathrm{d}A\, H_z(x, y)$, $\mathcal{H}_z = H_z(x = -d/2, y = -d/2)$ [24].

For small $|\vec{k}| \ll 1/d$ the standard definition of $\epsilon_{\mathrm{eff}} = \mathcal{D}_x/\mathcal{E}_x = \mathcal{D}_y/\mathcal{E}_y$ exactly coincides with that of ϵ_{qs} as explained in section 3.1. Therefore, $\epsilon_{\mathrm{qs}}(\omega)$ computed from equation (7) replaces ϵ_{eff} in equations (10). Assuming a planar wave with a wavenumber $\vec{k}$, it is found from equation (10) that two distinct classes of modes are supported by the medium: (a) longitudinal modes with $\vec{\mathcal{E}} \parallel \vec{k}$, and (b) transverse modes with $\vec{\mathcal{E}} \perp \vec{k}$. We refer to the longitudinal waves as bulk plasmons (BPs) and the transverse ones as plasmon polaritons (PPs). The dispersion relation for a BP is $\omega(\vec{k}) \equiv \omega_i^{(\mathrm{c})}$. Thus the cut-off frequencies also coincide with those of the BPs. For example, $\omega_1^{(\mathrm{c})}$ almost exactly coincides with the frequency (evaluated at the Γ-point) of the longitudinal resonance E_x shown in figure 1. The small difference is due to the finite ratio of d/λ. The dispersion relation for a PP is $|\vec{k}|^2 = \epsilon_{\mathrm{qs}}\omega^2/c^2$.

The frequency bands between the cut-offs and resonances define the non-resonant propagation bands of the PPs. From figure 3(d), there are four propagation bands (where $\epsilon_{\mathrm{qs}} > 0$) predicted by the quasi-static theory for $\omega < \omega_{\mathrm{p}}$. The first propagation band is fairly broad, extending from $\omega = 0$ to $\omega_1^{(\mathrm{r})} = 0.38\omega_{\mathrm{p}}$. The second band is very narrow: between $\omega_1^{(\mathrm{c})} = 0.61\omega_{\mathrm{p}}$ and $\omega_2^{(\mathrm{r})} = 0.63\omega_{\mathrm{p}}$. This band is 'sandwiched' between two electrostatic resonance curves shown in figure 1: longitudinal resonance E_x and transverse resonance E_y. Two modes exist inside the band: a BP with $\omega(\vec{k}) = \omega_1^{(\mathrm{c})}$ and a PP. These propagation bands are also revealed by the full electromagnetic simulation of equations (1), (2), and are shown in figure 2 (circles) to be in a very good agreement with the prediction of the QSED theory (solid curves). The third, also very narrow, propagation band is between $\omega_2^{(\mathrm{c})} = 0.77\omega_{\mathrm{p}}$ and $\omega_3^{(\mathrm{r})} = 0.79\omega_{\mathrm{p}}$, and it also supports a non-propagating BP and a propagating PP. The fourth band extends upwards in frequency from $\omega_3^{(\mathrm{c})} = 0.93\omega_{\mathrm{p}}$. None of the four propagation bands are revealed by the approximate electrostatic calculation which resulted in the band structure shown in figure 1.

3.3. Duality theorem in a sub-wavelength plasmonic crystal: relation between cut-off and resonance frequencies

We have discovered that for a highly-symmetric square lattice the cut-off and resonance frequencies are related to each other by a simple formula: for each resonance frequency $\omega_j^{(\mathrm{r})}$ there exists a cut-off frequency $\omega_i^{(\mathrm{c})}$ for which $\epsilon(\omega_i^{(\mathrm{c})}) = 1/\epsilon(\omega_j^{(\mathrm{r})})$. Numerical calculation of the zeros of ϵ_{qs} from equation (7) accurately confirms the duality principle. The duality principle in an SPC is rigorously derived below.

First we review a related duality principle for the resonances of an isolated plasmonic nanocylinder of an arbitrary shape. Recall that equations (5) are simultaneously satisfied for the electrostatic potential ϕ and magnetic field H_{qs}. Because the electric field is *normal* to $\phi = \mathrm{const}$ lines and *along* the $H_{\mathrm{qs}} = \mathrm{const}$ lines, equations (5) simply illustrate that in electrostatics there are two equivalent descriptions of the electric field: using potentials and field lines. Both H_{qs} and ϕ must vanish far away from the cylinder. It follows from equations (5) that if a resonance is supported by a rod of an arbitrary transverse shape for $\epsilon = \epsilon_1$, then there exists another resonance for $\epsilon_2 = 1/\epsilon_1$ [25]. For the resonances with $\epsilon = \epsilon_1$ and $\epsilon = \epsilon_2$ electric field lines and potential iso-contours are simply interchanged. Hence, the duality principle for isolated nanorods: all electrostatic resonances occur for frequency pairs (ω_1, ω_2) such that $\epsilon(\omega_1) = \epsilon_1$ and $\epsilon(\omega_2) = 1/\epsilon_1$.

Symmetry considerations must be used for deriving a duality relation for a two-dimensional SPC. Let us assume that an electrostatic resonance is found for $\epsilon = \epsilon_1$ for a y-polarized electric field. The corresponding potential eigenfunction ϕ_1 is a solution of equation (5) and satisfies the following homogeneous conditions at the unit boundaries $(x, y) = (\pm d/2, \pm d/2)$: (a) ϕ_1 and its derivatives are periodic; (b) $\phi_1(y = \pm d/2) = 0$; (c) $\partial_x\phi_1(x = \pm d/2) = 0$. By symmetry, another eigenfunction $\tilde{\phi}_1$ obtained by a 90° spatial rotation of ϕ_1 also satisfies equation (5). Next, consider a pair of magnetic field functions $H_z^{E_x} = \phi_1$ and $H_z^{E_y} = \tilde{\phi}_1$, and the frequency ω_2 such that $\epsilon(\omega_2) = 1/\epsilon_1$. It follows from equation (5) that $H_z^{E_x}$ and $H_z^{E_y}$ both satisfy equation (1) in the quasi-static limit of $\omega^2 d^2/c^2 \ll 1$. Moreover, the periodic boundary conditions satisfied by $(H_z^{E_x}, H_z^{E_y})$ indicate that the pair are the magnetic fields of the BP and the PP at the cut-off point of $\vec{k} = 0$ (see equation (2)). Therefore, ω_2 is the cut-off frequency. The inverse is also true: if the cut-off frequency is ω_3, than there is a resonance at ω_4 such that $\epsilon(\omega_4) = 1/\epsilon(\omega_3)$.

Using a frequency-dependent label $s(\omega) = 1/(1 - \epsilon(\omega))$ (which reduces to $s(\omega) = \omega^2/\omega_{\mathrm{p}}^2$ for the plasmonic dielectric permittivity $\epsilon(\omega) = 1 - \omega_{\mathrm{p}}^2/\omega^2$), the duality condition can also be expressed as $s(\omega_i^{(\mathrm{r})}) + s(\omega_j^{(\mathrm{c})}) = 1$ (which reduces to $\omega_i^{2(\mathrm{r})} + \omega_j^{2(\mathrm{c})} = \omega_{\mathrm{p}}^2$ for the plasmonic ϵ). We have verified that, indeed, with high accuracy, $\omega_1^{(\mathrm{r})2} + \omega_3^{(\mathrm{c})2} = \omega_{\mathrm{p}}^2$, $\omega_2^{(\mathrm{r})2} + \omega_2^{(\mathrm{c})2} = \omega_{\mathrm{p}}^2$, and $\omega_3^{(\mathrm{r})2} + \omega_1^{(\mathrm{c})2} = \omega_{\mathrm{p}}^2$ for the particular plasmonic structure considered in this paper.

4. Propagation bands associated with electrostatic resonances: origin of negative refractive index

In section 3 the electromagnetic properties of the SPCs for frequencies sufficiently removed from higher multipole resonances were described using the quasi-static electric dipole theory. The justification for QSED theory is that the dipole scattering of incident electromagnetic waves by individual nanoparticles dominates over high-multipole scattering. This is not the case for frequencies very close to those of electrostatic multipole resonances [26]. For those frequencies multipolar scattering is resonantly enhanced, and can dominate over the dipolar scattering. That the QSED theory may be inadequate for describing all propagating modes in an SPC becomes apparent by noting that the propagation band marked by triangles in figure 2 belongs to the frequency range where $\epsilon_{\mathrm{qs}} < 0$. Therefore, in the vicinity of the A_2 electrostatic resonance the QSED description breaks down, and the resonant frequency broadens into a frequency band with a finite group velocity $\vec{v}_{\mathrm{g}} = \partial\omega/\partial\vec{k}$.

Moreover, we show that an SPC can also exhibit a finite magnetization, i.e. $\vec{\mathcal{B}} \neq \vec{\mathcal{H}}$. Whether or not finite magnetization exists depends on the azimuthal dependence of the resonant field. Here we concentrate on the A_2 resonance. Recall that in the vicinity of electrostatic resonance $H_z = H_{\rm qs} + H_1$, where $H_{\rm qs}$ is responsible for the electrostatic (potential) portion of the electric field, and H_1 is perturbatively calculated using equation (4). Although the electric field near resonance is mostly electrostatic, it possesses a non-vanishing solenoidal component:

$$\vec{E} = -\vec{\nabla}\phi + \vec{S}, \tag{11}$$

where $\vec{S}$ is a purely solenoidal field $\vec{\nabla}\cdot\vec{S} = 0$, and ϕ, $\vec{S}$ satisfy

$$\vec{\nabla}\times\vec{S} = \mathrm{i}\frac{\omega}{c}H_{\rm qs}\vec{e}_z \qquad \text{and}$$

$$-\nabla^2\phi \approx \mathrm{i}\frac{c}{\omega}\vec{e}_z\cdot\left(\vec{\nabla}\epsilon^{-1}\times\vec{\nabla}H_{\rm qs}\right). \tag{12}$$

It is this small (to order $\omega^2 d^2/c^2$) solenoidal part of the electric field that is responsible for the magnetic properties of an SPC. Those magnetic properties can manifest themselves as the negative magnetic permeability in the vicinity of an electrostatic resonance, and give rise to the negative refractive index [15].

The magnetic permeability $\mu_{\rm eff}$ is affected because the A_2 mode carries the electric current which produces a finite magnetic moment. The electrostatic $\vec{E}$-field of the mode inside the plasmonic rod is derived from the electrostatic potential

$$\phi = \sum_{n=1}^{\infty}\Phi_n^{(A_2)}\left(\frac{r}{R}\right)^{4n}\sin 4n\theta. \tag{13}$$

The electric field lines correspond to the iso-contours of the quasi-static magnetic field given by

$$H_{\rm qs} = \sum_{n=1}^{\infty}H_n^{(A_2)}\left(\frac{r}{R}\right)^{4n}\cos 4n\theta. \tag{14}$$

The expansion coefficients $\Phi_n^{(A_2)}$ and $H_n^{(A_2)}$ are found numerically by solving equations (5) with periodic boundary conditions. Although we label the electromagnetic modes according to the spatial symmetry of their electrostatic potential, note from equations (13), (14) that the electrostatic potential and the magnetic field transform according to the A_2 and A_1 irreducible representations, respectively. This is a general property of square (and hexagonal) SPCs: ϕ and $H_{\rm qs}$ belong to the complimentary irreducible representations.

The monopole term $H_0^{(A_2)}$ does not contribute to the electrostatic field in the quasi-static limit. However, for a finite particle size there is a non-vanishing solenoidal electric field according to equations (11), (12). By Stokes' theorem, the azimuthal electric field inside the particle is found from $2\pi r E_\theta = \mathrm{i}(\pi r^2)H_0^{(A_2)}\omega/c$ to be $E_\theta = \mathrm{i}(\omega r/2c)H_0^{(A_2)}$. The corresponding electric current in the plasmonic rod is given by $J_\theta = -H_0^{(A_2)}\omega^2 r/2c^2\times(\epsilon-1)$. This current produces a magnetic moment density $\vec{M} = (1/2c)\langle\vec{r}\times\vec{e}_\theta J_\theta\rangle$, where the average is taken over the unit cell. After straightforward algebra we obtain $M = (pH_0^{(A_2)}/16\pi)(1-\epsilon)\omega^2R^2/c^2$. The magnitude of the induced magnetic moment depends on two factors: the particle size (through the ω^2R^2/c^2 term) and the interparticle proximity (through the value of $H_0^{(A_2)}$ which rapidly decreases as a function of R/d).

We have calculated the effective permittivity $\epsilon_{\rm eff}$ and permeability $\mu_{\rm eff}$ using the procedure explained in section 3.2. Both $\epsilon_{\rm eff}$ and $\mu_{\rm eff}$ have been calculated for a range of wavenumbers $\vec{k} = k\vec{e}_x$ and the corresponding frequencies $\omega(k)$. For $kd \ll \pi$ it follows from the analyticity of $\omega(\vec{k})$ that the frequency depends only on $|\vec{k}|$ and not on its direction. For $k_0 = 0.6/d$ and $\omega_0 = 0.6\omega_{\rm p}$ (or $n_{\rm eff} = -1$) we numerically computed that $\mu_{\rm eff} = -2.35$ and $\epsilon_{\rm eff} = -0.427$. Therefore, at this frequency our SPC can be viewed as a doubly-negative material. This is consistent with the negative group velocity of the A_2 wave. Note that the hybridized monopole/octupole resonance affects not only the magnetic permeability of the SPC, but also the dielectric permittivity: the effective medium calculation using equation (7) yields $\epsilon_{\rm qs}(\omega_0) = -0.65$ that is significantly different from $\epsilon_{\rm eff}$.

It is this negative $\mu_{\rm eff}$ that enables wave propagation in the region where $\epsilon_{\rm qs} < 0$, and the QSED theory prohibits wave propagation. We have found numerically that an electromagnetic wave with the frequency inside the A_2 band incident from vacuum onto an SPC can couple into the crystal with very little reflection. Moreover, we observed strong enhancement of the field amplitude inside the crystal. This enhancement is caused by the very low group velocity of the A_2 band. In section 5 we speculate how the flatness of this band and its proximity to the plasmon polariton band can be employed to improve the surface-enhanced Raman scattering.

5. Applications of SPCs to surface-enhanced Raman scattering

The close proximity of the two flat propagation bands of a two-dimensional SPC shown in figure 2 (labelled by circles and triangles) may be useful for surface-enhanced Raman scattering (SERS) [27]. Arrays of closely-spaced nanoparticles are known to cause a significant enhancement of the local fields with respect to the incident laser field: $R = E_{\rm local}/E_{\rm inc} \gg 1$ [17, 28, 29]. This enhancement is caused by coupling to the narrow electrostatic (plasmon) resonance. The narrower the resonance ($\delta\omega = \omega_1/Q$, where $Q \gg 1$ is the quality factor) is, the higher the enhancement. Molecules placed in the region of the enhanced incident field with frequency ω_1 re-emit at the Raman-shifted frequency $\omega_2 = \omega_1 - \Omega_{\rm v}$, where $\Omega_{\rm v}$ is the vibrational frequency of interest. The spectacular enhancements of the Raman signal observed in the experiments [27] are related to the fact that electromagnetic fields at both ω_1 and ω_2 are enhanced by the structure. Only in that case the enhancement of the Raman signal scales as R^4. The field enhancement R is proportional to Q. The exact proportionality coefficient can substantially exceed unity for nanoparticles with sharp features (for example, prisms with sharp corners or almost-touching nanospheres).

The implication of both the emitted and absorbed light being inside the resonance curve is that $\omega_1 - \omega_2 < 1/Q$, or that $Q < \Omega_{\rm v}/\omega_1$. Because the Raman enhancement scales as R^4, the largest electromagnetic enhancement is proportional to $(\omega_1/\Omega_{\rm v})^4$. This estimate puts an upper limit on the vibrational frequencies that can be detected with SERS while still enjoying the enhancement benefits. For example, for $\Omega_{\rm v} = 1000$ and $\omega_1 = 30\,000$ cm^{-1} (corresponding to $\lambda_1 = 350$ nm) the

electromagnetic Raman signal enhancement is only of order 10^6. Although higher enhancements have been reported, they are primarily found in the narrow gap between dimer-forming nanoparticles [27]. If the separation between the Stokes and fundamental frequencies is larger than ω_1/Q, these dramatic enhancements of the Raman signal cannot be realized.

Our suggestion is to employ two well separated propagation bands, each of which is very flat. If each of the bands has the spectral width of $(\delta\omega_1)$ and $(\delta\omega_2)$, and the frequency separation between the bands is $\Omega_v \gg (\delta\omega_{1,2})$, then these two bands can be employed for detecting the vibrational frequency Ω_v. The band separation can be easily tuned by changing the rods' radii R and, possibly, their shapes. The magnitude of the signal enhancement is governed by the width of each individual band $(\delta\omega_{1,2})$ while the detected vibrational frequency is governed by the separation between the bands. One example of such closely located flat bands is shown in figure 2 (two upper bands marked by triangles and circles).

Acknowledgments

This work is supported by the NSF's Nanoscale Exploratory Research Contract No. DMI-0304660 and by the ARO's MURI program 4F-01541.

References

[1] Yablonovich E 1987 *Phys. Rev. Lett.* **58** 2059
[2] John S 1987 *Phys. Rev. Lett.* **58** 2486
[3] Joannopoulos J D, Meade R D and Winn J N 1995 *Photonic Crystals: Molding the Flow of Light* (Princeton, NJ: Princeton University Press)
[4] Yablonovich E 1994 *J. Mod. Opt.* **41** 173
[5] Solli D R, McCornick C F, Chiao R Y and Hickmann J M 2003 *Opt. Express* **11** 125
[6] Urzhumov Y A and Shvets G 2003 *Proc. SPIE* **5184** 47
[7] Cregan R F, Mangan B J, Knight J C, Birks T A, Russell P St J, Roberts P J and Allan D C 1999 *Science* **285** 1537
[8] Painter O, Lee R K, Scherer A, Yariv A, O'Brien J D, Dapcus P D and Kim I 1999 *Science* **284** 1819
[9] Luo C, Johnson S G, Joannopoulos J D and Pendry J B 2003 **68** 045115
[10] Smith D R, Schurig D, Rosenbluth M, Schultz S, Ramakrishna S A and Pendry J B 2003 *Appl. Phys. Lett.* **82** 1506
[11] O'Brien S and Pendry J B 2002 *J. Phys.: Condens. Matter* **14** 4035
[12] Moroz A 2000 *Europhys. Lett.* **50** 466
[13] McGurn A R and Maradudin A A 1993 *Phys. Rev.* B **48** 17576
[14] Huber T E and Luo L 1997 *Appl. Phys. Lett.* **70** 2502
[15] Smith D R, Padilla W J, Vier D C, Nemat-Nasser S C and Schultz S 2000 *Phys. Rev. Lett.* **84** 4184
[16] Pendry J B 2000 *Phys. Rev. Lett.* **85** 3966
[17] Genov D A, Sarychev A K, Shalaev V M and Wei A 2004 *Nano Lett.* **4** 153
[18] Bergman D J and Stroud D 1992 *Solid State Phys.* **46** 147
[19] Stockman M I, Faleev S V and Bergman D J 2001 *Phys. Rev. Lett.* **87** 167401
[20] Smith D R, Vier D C, Kroll N and Schultz S 2000 *Appl. Phys. Lett.* **77** 2246
[21] FEMLAB Reference Manual 2003 Version 2.3, Comsol AB, Sweden
[22] Lyubarskii G Y 1960 *Application of Group Theory in Physics* (New York: Pergamon)
[23] Landau L D and Lifshitz E M 1975 *Electrodynamics of Continuous Medium* (New York: Pergamon)
[24] Pendry J B, Holden A J, Robbins D J and Stewart W J 1999 *IEEE Trans. Microw. Theory Tech.* **47** 2075
[25] Fredkin D R and Mayergoyz I D 2003 *Phys. Rev. Lett.* **91** 253902
[26] Agranovich V M 1984 *Crystal Optics with Spatial Dispersion, and Excitons* (Berlin: Springer)
[27] Michaels A M, Jiang J and Brus L 2000 *J. Phys. Chem.* B **104** 11965
[28] Li K, Stockman M I and Bergman D J 2003 *Phys. Rev. Lett.* **91** 227402
[29] Garcia-Vidal F J and Pendry J B 1996 *Phys. Rev. Lett.* **77** 1163